High energy X-ray diffraction as a method of strain analysis

Shu Yan Zhang[1], Alexander M. Korsunsky[2]

[1] ISIS Facility, Science and Technology Facilities Council, Rutherford Appleton Laboratory, Chilton, Didcot, UK OX11 0QX. Tel: +44 12354455011 Fax: +44 1235445720
Email:s.y.zhang@rl.ac.uk

[2]Dept of Engineering Science, University of Oxford, Parks Road, Oxford UK OX1 3PJ

Abstract

Strain analysis in engineering components and assemblies is important for the purposes of evaluating deformation response to in service or laboratory loading, so as to characterise the presence of flaws or damage, and also of residual stresses that affect engineering performance. Synchrotron radiation provides brightest (most parallel and high intensity) X-ray beams over a wide rage of energies. Higher energy X-rays are particularly well-suited for the analysis of internal strains within bulk (poly)crystalline materials, because of their excellent penetration depths exceeding ten(s) of millimetres in most structural alloys. Experimental modes (monochromatic and energy-dispersive) will be reviewed, and information obtainable from diffraction patterns (inter-granular and macro-strains, texture) will be illustrated. The connection between diffraction analysis of internal strains and fatigue durability will be pointed out.

1. Introduction: experimental strain analysis and structural design

The history of human civilisation to a significant part is the history of man's increasing ability to control and re-shape the material world that surrounds him: making utensils, tools and weapons; building dwellings, roads and bridges; inventing and implementing devices to heavy lifting, fast travel, digging deep or rising high. In all these endeavours experiment and thought go hand in hand. When ideas conceived in a man's mind become implemented in wood, stone or metal, the resulting structures can then be used and observed in service. Information is then collected on their convenience, safety and reliability. This opens up possibilities for design modifications, changes and improvements.

The central function of all load-bearing structures is to sustain stress. Usually there is a requirement to do so without failure or excessive deformation, although in some cases this is allowed or even intended (consider, for example, the function of plastic hinges or car crumple zones). Since no material may ever possess infinite stiffness, sustaining stress goes hand in hand with experiencing deformation, i.e. strain. Stress, expressed in the units of force per cross-sectional area, has been widely accepted as a convenient concept for engineers and designers, ever since Leonardo observed in his experiments with cantilevered beams that neither load nor cross-sectional area on their own provide a useful measure of

material strength. Thus, the significance of stress inhomogeneity was identified. However, stress is an imaginary quantity that is very difficult to measure directly, and that is also strongly dependent on the scale of consideration.

Strain, in simple engineering terms, is defined as the ratio of elongation to initial length, or relative change of angle due to shear. Naturally, the definition of strain is also dependent on scale, although it can be argued that its relationship with the physical quantities such as displacement is more direct. Furthermore, an arsenal of strain measurement techniques has evolved over decades, and is widely employed in the experimental studies of deformation behaviour of materials and structures. The significance of this activity is to characterise the response to applied loads, particularly such that correspond to in-service loading; and to observe the response of objects so as to predict the integrity of various designs. This is the principal significance of strain analysis for structural design.

2. A brief overview of experimental methods of strain analysis

An important observation that arises in the analysis of strains is that strains are composed of the elastic and inelastic parts, i.e.

$$\varepsilon = \varepsilon_{el} + \varepsilon_{inel} \quad \text{.....(1)}$$

where ε_{inel} includes thermal strains, plasticity, creep, transformation-induced strains, etc.

The analysis of stress evolution in response to deformation, and the analysis of residual stresses both depend crucially on the partitioning of strain into elastic and inelastic parts. In fact, in numerical simulation of complex material deformation the crucial task of the modeller is to specify how strain (or its small increment during loading is partitioned between elastic and inelastic parts. Once this partitioning is carried out, the elastic part determines the stress through the appropriate version of Hooke's law (3D, plane stress or plane strain; isotropic or anisotropic), while the inelastic part defines material state through internal variables that pertain to hardening, back stress, damage, etc.

Experimental methods of strain evaluation can be divided into contact and non-contact (or optical). In a contact method, a device is attached to the sample that is being deformed that needs to have deformation resistance that is considerably lower than the sample, so that its deformation follows that of the sample. The device is instrumented in a way that produces a signal proportional to the average value of strain over the span of the device. This signal can then be calibrated, and *total strain* evolution recorded on the computer as a function of deformation time, applied load, etc.

Most prominent examples of the contact method are a resistive strain gauge and a clip gauge. A resistive strain gauge consists of a serpentine-like pattern of thin metallic wire with parallel lengths aligned with the direction of the strain being measured. The wire material has low temperature-resistance coefficient, but responds to small changes in length and cross-section by changing its resistance. This can be picked up electronically, amplified and converted into a voltage signal that can be calibrated to provide a strain reading. Strain gauges fail by debonding or tearing at larger strains, but allow accurate measurements in the elastic and early elastic-plastic deformation regimes (particularly for metals). A clip gauge consists of a pair of knife edges that are attached to two positions on the sample

separated by a well-known gauge length, either by gluing or e.g. with the help of rubber bands. Between the two attachment points the clip gauge usually has a flexible element that itself suffers deformation that scales linearly with extension, and generates an electrical signal for recording. Resistive strain gauges are often used for this purpose. The drawback of the contact methods consist in the necessity of preparing the surface and establishing contact with the specimen (not suitable for sensitive samples, problematic at high temperatures). Furthermore, the possibility of conducting multi-point distributed field measurements is limited.

Contact methods only allow the measurement of strain with respect to a reference state, and thus on their own have limited utility for residual strain evaluation. However, they can be used in combination with destructive or semi-destructive methods involving material removal to measure strain increment due to stress/strain redistribution (hole drilling, slitting, sectioning), so that prior residual state can be assessed via the application of a model. A further contact method of measuring *displacements* deserves a mention, namely, touch probe method involving the use of coordinate measurement machines. This allows evaluation of deflection and distortion, but cannot provide point tracking without additional provision of reference markers on the specimen.

Non-contact (optical) methods lend themselves very well to full field measurement. Photoelastic methods rely on the birefringence of special coating applied to the sample, and the calculation of phase of polarised light through interference between the reflected and reference beams. Speckle interferometric techniques employ a similar principle, but can in principle be used without sample surface preparation (although in practice the application of paint may be needed). Finally, digital image correlation techniques employ statistical matching between pixel regions to find the most probable displacement between deformed and reference configurations. All these methods assess *total strain* and can also be used in combination with destructive methods to evaluate residual states.

Most conventional methods of strain evaluation struggle to make a distinction between elastic and inelastic strains, since they measure *total strain*. While such measurements are clearly useful in the study of material deformation and can be compared with the predictions of simulations, since they do not separate the elastic part of strain readily, straightforward stress calculation is not possible. Diffraction methods occupy a special place in strain analysis precisely for the reason that they are capable of providing a measure of *elastic* component of strain alone, and thus offer a firm basis for stress evaluation (including residual stress).

3. Diffraction methods

Engineering strain measurement by neutron diffraction has developed from the pioneering work at Harwell in the early 1980's [1] and subsequently at Institute Laue Langevin (ILL). The first instruments used were modified triple-axis spectrometers and a two-axis powder diffractometer. In the early 1990's there was an upsurge in the design of dedicated strain scanning instruments and the development of synchrotron X-ray sources made available X-ray beams millions of times more powerful than laboratory X-ray sources [2]. This decade has witnessed a significant increase in residual stress evaluation using diffraction of

penetrating radiation, such as neutrons or high energy X-rays. They provide a powerful non-destructive method for determining the level of residual stress in engineering components through precise characterisation of interplanar crystal lattice spacing.

Residual stresses and prior deformation (e.g. during fabrication) experienced by structural components can exert a strong influence on the deformation behaviour, and hence durability of engineering structural components. The unique non-destructive nature of these measurement techniques is particularly beneficial in the context of engineering design, since it allows the evaluation of a variety of structural and deformational parameters inside real components without the need to remove any materials, or, at worst, with minimal interference [3].

X-ray and neutron stress analysis share many common features. They use Bragg's Law as the underlying diffraction equation. The measured crystalline lattice is used as an atomic strain gauge and the approaches to estimate the strain-free lattice spacing are the same. The principles for setting up the experiment and data interpretation approaches are similar. Laboratory X-ray diffraction is a well-established technique for surface measurement, but the penetration depth is very shallow. As reported in [4], the penetration depth into steel of the characteristic radiation from a Cu-Kα source is 0.004mm, while the penetration depth for Aluminum is 0.075mm. Synchrotron X-ray and Synchrotron X-ray and neutron are equally appropriate for both macro- and microstresses for the bulk of materials and components and can penetrate hundreds/ thousands times deeper than the laboratory X-rays, benefiting from their high penetrating power. Due to the differences in absorption, beam flux and divergence of the beam, X-ray and neutron stress analysis are viewed as complementary techniques. Neutron strain scanning is preferred where large path lengths are involved, especially for components comprising high atomic number materials. Synchrotron X-ray instruments are generally offer higher spatial resolution (down to micro levels) and higher data acquisition rates (as fast as sub-second), especially in light materials. They are particularly appropriate for the study of coated systems and plate samples. This paper will focus on the stress analysis using synchrotron X-ray diffraction, which is a technique offers high penetration, high flux and low beam divergence, combined with excellent spatial resolution.

The principle of diffraction strain measurement in polycrystalline alloys relies on Bragg's law that establishes the relationship between the average interplanar lattice spacing d within the sampling (or gauge) volume, on the one hand, and the wavelength (or energy) of X-ray photons and their scattering angle 2θ, on the other:

$$n\lambda = 2d\sin\theta \quad \text{.....(2)}$$

where λ is wavelength, d inter-planar spacing, θ half diffraction angle, n reflection order.

When a polycrystalline aggregate is deformed elastically, inter-planar spacing within constituent grains changes. Within a set of planes that have similar orientation with respect to the stress direction, the inter-planar spacing is essentially similar between one grain and another. This grain-set-specific strain causes observable shifts of diffraction peaks. Only elastic strain is accommodated within the deformation, therefore this shift is purely a measure of the elastic strain. (Note that plastic strain is accommodated by dislocation glide through crystals. This deformation does not change the average lattice spacing. However, the presence of increasingly dense distributions of dislocations broadens the spread of

strains around the average value determined by elastic deformation, and manifests itself in diffraction peak broadening). As only those grains that possess orientations that fulfill the criteria of Bragg reflection will contribute to the measured reflection, the strain obtained will be representative of the average strain from grains within the irradiated volume [5]. Strain can be found from deformed lattice spacing d as

$$\varepsilon = \frac{(d - d_0)}{d_0} = \frac{\Delta d}{d_0} \quad \text{.....(3)}$$

where d_0 denotes unstrained lattice spacing. Since it is possible to consider the positions of individual diffraction peaks, their shifts can be interpreted in terms of lattice deformation along selected directions within the crystal(s) and with respect to the laboratory system. This approach allows additional light to be shed on the mechanics of polycrystal deformation.

In practice the determination of interplanar spacing can be carried out in one of two distinct modes: angular dispersive mode using a fixed wavelength measuring the angular shift of a diffracted peak by scanning angles; and energy dispersive mode using white radiation detected by an energy-resolving detector at a fixed angle. In angular dispersive mode, monochromatic beams with narrow bandwidths of photon energy or wavelengths are required. The energy resolution ($\Delta E/E$) of the monochromatic beam is usually in the range of 10^{-3} to 10^{-4}. Monochromatic X-ray beam diffraction allows accurate determination of diffraction peak intensities, shapes, and positions. These diffraction patterns are either recorded using a detector scanning over a range of the diffraction scattering angle, or with a position-sensitive detector capable of registering the distribution of photon flux along a line or across a two-dimensional surface.

In the energy dispersive mode, a white beam is used and the diffraction pattern is recorded by means of solid state semiconducting detectors. The white beam mode provides a very high counting efficiency as a much broader bandwidth is used to collect multiple reflections simultaneously. A whole diffraction pattern is obtained at a constant diffraction angle within a comparatively short time, whereas the angle dispersive mode with point detector requires significantly longer counting times to collect the data from comparable sections of the diffraction pattern, owing to a reduced photon flux (due to monochromation) and because of the need for detector scanning.

The energy dispersive mode offers fast data collection, but the energy resolution ($\Delta E/E$) of the detectors is typically of the order of 10^{-2}, since the diffraction peak shape definition is particularly limited by the resolution of the energy-dispersive (ED) detector used. Nevertheless, the overall photon counts are potentially several orders of magnitude greater than those for monochromatic beams. Simultaneous collection of information about scattered intensity across a wide range of energies results in a diffraction pattern (that can be converted to intensity vs lattice spacing pattern using appropriate calibration, [6-9]) allows subsequent data interpretation that involves the refinement of a crystal lattice and scattering model (Rietveld refinement) through non-linear least squares fitting to the entire pattern containing multiple diffraction peaks. This allows the determination of average lattice parameters (e.g. a, c). Hence, the accuracy of the measurement can be significantly improved by using an appropriate analysis, such as a whole pattern refinement, where the

simultaneous use of multiple peak positions allows the lattice parameters to be determined to a degree of accuracy better than 10^{-4}.

Measurement arrangements and experimental studies described below demonstrate the capabilities of evaluating residual strains (and ultimately stresses) white beam high energy X-ray diffraction.

4. Case studies

4.1 Shot peened steel plates

The objective of this case study was to investigate the effect of varying shot-peening intensities and material thickness on the residual stress. Intensities investigated were Almen 3A and 6A. For this study five stainless steel strips were used. Samples differed in terms of the peening intensity and thickness (Table 1).

Table 1. Sample description

Sample description	Peening intensity: 3A (Pressure: 4 psi; Distance: ± 266mm; Impact angle: 90^o)	Peening intensity: 6A (Pressure: 9 psi; Distance: ± 228mm; Impact angle: 90^o)
Almen strip, 1.3mm		AP2YZ
174-PH, 1.3mm	BP1YZ	BP2YZ
174-PH, 5mm	T5P1YZ	T5P2YZ

Synchrotron X-ray scattering experiments were carried out at the UK Daresbury Synchrotron Radiation Source (SRS), on Station 16.3. The experiment was performed in the white beam energy dispersive mode, which allowed multiple Bragg peaks to be measured simultaneously. Samples were scanned through a rectangular beam that an aperture of 0.1mm along the peening depth. To extract the information about inelastic deformation during shot peening treatment of sample surfaces, the residual elastic strain (r.e.s.) profiles measured by diffraction are presented and analysed below.

Fig. 1 illustrates the data for samples of the same material and same thickness, but with different peening intensity. It is clear that varying the peening intensity induces changes in the *magnitude* of eigenstrains and residual elastic strains, as well as their *depth*, and the magnitude of the reactive bending strains and the strains in the reverse plastic flow region near the back face. Higher peening intensity leads to larger residual elastic strains.

Three regions are identified: peen-induced plasticity, elastic bending region and bending-induced reverse plastic deformation at the back face. Consideration of the profile from BP1YZ allows these three regions to be identified. In the vicinity of the sample surface ($x = 0$) a layer of compressive strain about 0.2mm deep is found, with maximum compressive residual strain of about 800 microstrain (800×10^{-6}). This region arises directly due to local plastic deformation induced by peening impact. Compressive residual elastic strain arises in response to the tensile eigenstrain component parallel to the peened surface. Near surface residual compression is counter-acted by the bending stresses that develop in the work piece. These vary linearly across sample thickness, and are sufficient to equilibrate resultant longitudinal stress and moment. The region of linear variation of r.e.s. due to bending reaction extends from about 0.2mm to 0.75mm from the peened surface.

It is sometimes observed in samples subjected to surface treatment of sufficient intensity that inelastic deformation is caused not only at the 'front', directly treated surface, but also on the 'back' face. This may be caused by the deformation associated with the development of bending reaction stresses. These strains vary linearly through the sample. They reach maximum values at the opposite 'back' face, and may cause additional plastic deformation. Note that their magnitude near the 'front' face is moderated by the presence of eigenstrain induced by peening, or by some similar process. In Fig. 1 the region of 'reverse' plastic flow at the 'back' face lies between 0.75mm depth from the peened face and the back face.

As sample bends in response to peening eigenstrains, the strain profile presents the combination of elastic bending (linear with distance) and remaining residual compression near the peened surface due to permanent stretching induced by shot impact. Then peening-induced plastic strain profile can be obtained by subtracting the complete r.e.s. curve from the straight line fitted to elastic bending profile observed below the surface treated layer.

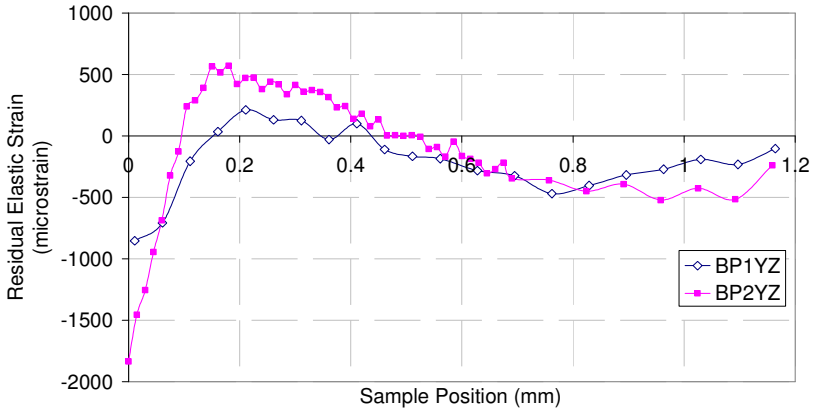

Figure 1 R.e.s. profiles for samples of the same material and thickness, but different peening intensity

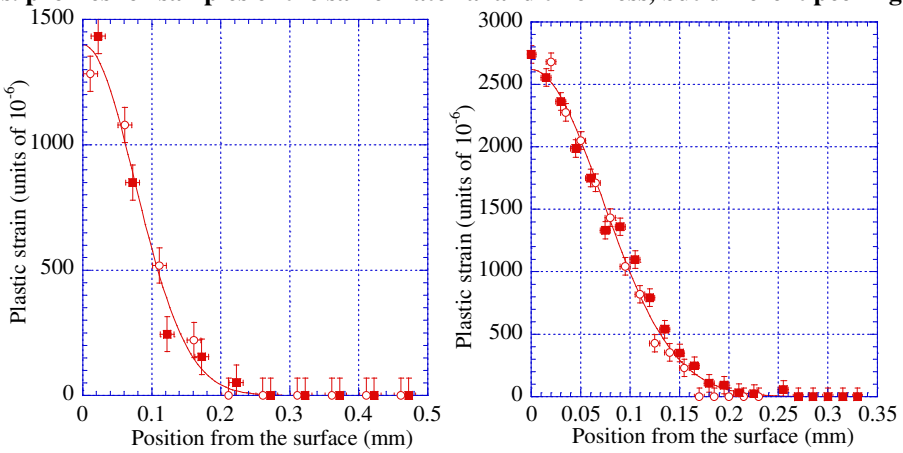

Figure 2 (a). Plastic strain profile for intensity 3A. (b). Plastic strain profile for intensity 6A.

4.2 Shot peened wedge coupon from an aeroengine fanblade

A shot peened wedge coupon from a Ti-6Al-4V aeroengine fan blade was studied. Prior to peening, the blade was made by diffusion bonding of three layers of Ti alloy (two skins and the line core layer). It is therefore interesting to know the strain distribution, both near-surface and across bonded layers. The sample was examined on Station 16.3 at SRS. The

experiment was performed in the white beam energy dispersive mode. Strains ε_{yy} and ε_{xx} were measured along 11 lines across the thickness of the blade, spaced by 3mm. The mapped region is shown in Fig 3. Beamsize of 0.2mm (in y) × 0.04mm (in x) and step size of 0.04mm (in x) were selected. Fig. 4 illustrates the ε_{xx} and ε_{yy} strain maps. Peen-induced plasticity (about 0.2mm from the surface) is evident, illustrating how synchrotron strain measurement can provide high spatial resolution.

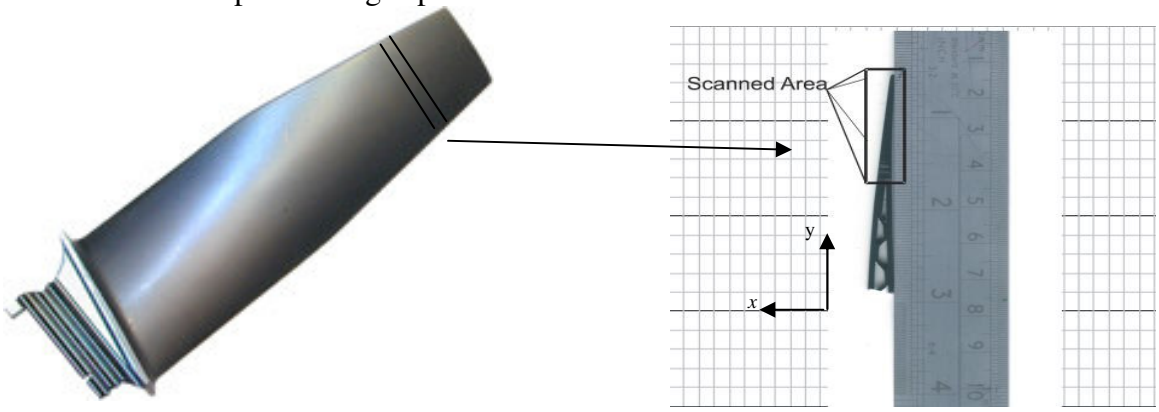

Figure 3. Edge of Ti-6Al-4V alloy fan blade

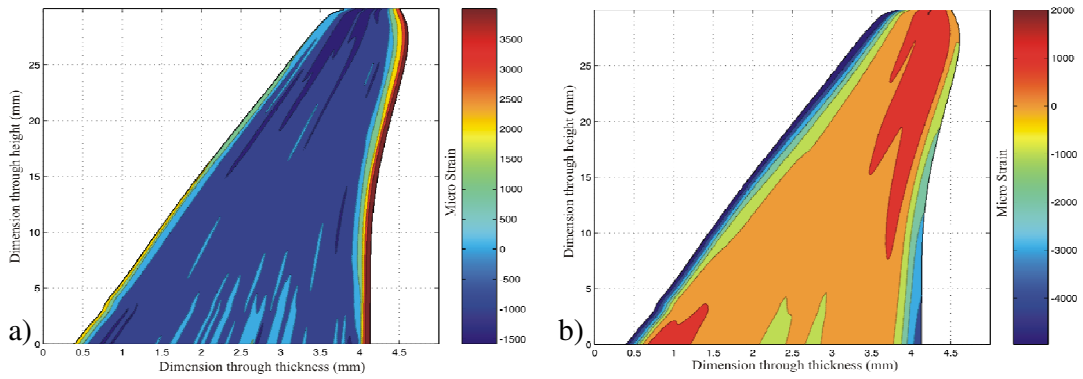

Figure 4. Elastic residual strain profile presented in the blade section a) ε_{xx} b) ε_{yy}

4.3 Laser bent plate

This study addressed residual elastic strains in mild steel plates bent by multi-pass laser forming process (three scans). Synchrotron ED X-ray diffraction was used to carry out strain mapping at Station 16.3 at SRS. The study sample was a strip extracted from the plane normal to laser beam travel to study residual stress distribution due to laser treatment.

Fig. 5 shows the through-thickness residual elastic strain ε_{xx} that varies approximately between 450 and –200 microstrain. The greatest tensile strain of 445 microstrain arises at the near-surface region where laser heating effect was most pronounced. Near surface tensile strain decays over a depth of 1.15 mm and then gradually becomes compressive, until reaching a maximum value of -167 microstrain approximately halfway into the steel plate, 2.5 mm below the surface. With depth into the specimen the strain becomes tensile again and ends off in compression of about -200 microstrain at the rear face of the plate.

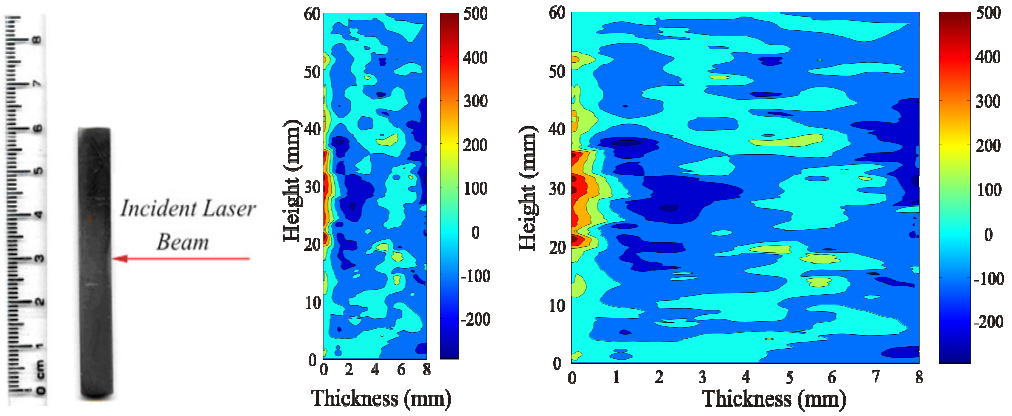

Figure 5. Geometry and measured r.e.s. component ε_{xx} in the through-thickness slice of the steel plate.

4.4 Thermal spray coatings

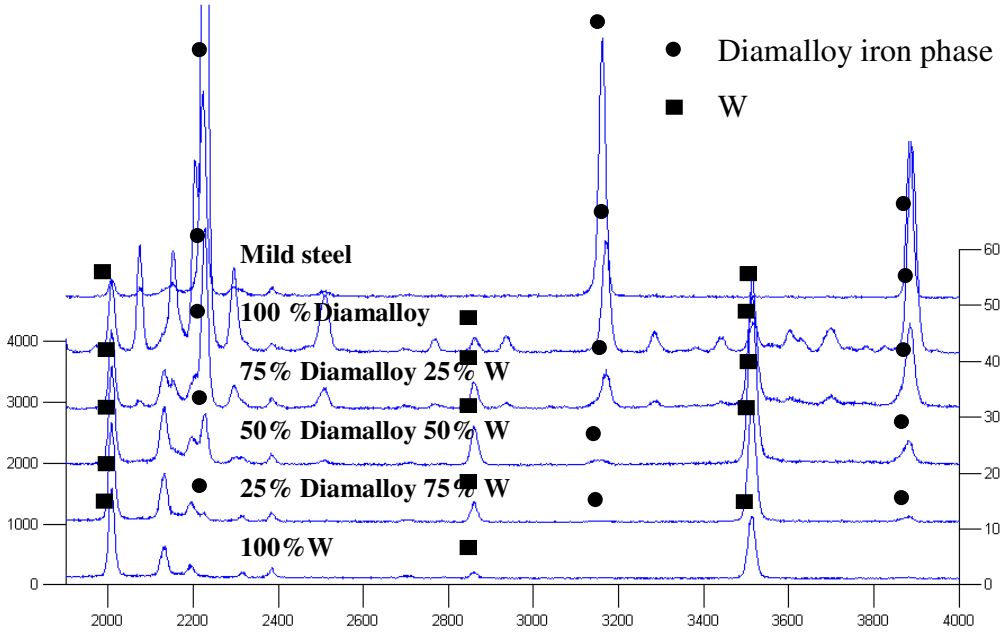

Figure 6. Examples of diffraction pattern from the coating to the substrate of sample VPS 128b.

A coating system produced by vacuum plasma sprayed coating technique was characterized in terms of the r.e.s. Two samples with different morphologies of coating were used. First sample (128b) has a 0.5-0.6mm thick functionally gradient coating comprising five graded layers on a 5mm-thick mild steel substrate. FGM-coatings were produced as follows. Mild steel substrates were first coated with a bond layer, using 100% Diamalloy 1008 (denoted D below) powder. Compositionally graded layers then deposited, namely: 100% D, 75% D + 25% W, 50% D + 50% W, 25% D + 75% W, and 100% W. The other sample (164b) has a thick (~2mm) layer of VPS W on 5mm thick surfi-sculpt 316L stainless steel. Measurements were performed in the white beam energy dispersive mode with twin-detector setup at the high energy synchrotron beamline ID15 at ESRF. Strains longitudinal

(ε_{xx}) and transverse to the coating surface (ε_{yy}) were measured simultaneously as line scans through coating to the mild steel surface. 2D strain maps around bond coat were examined. Measurements on VPS 128b with FGM coating also showed phase fraction changes (Fig 6).

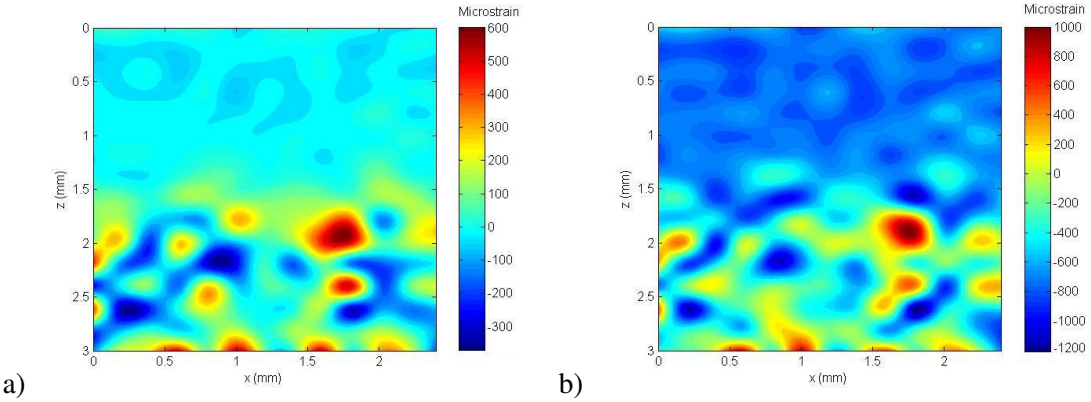

a) b)

Figure 7. VPS 164b strain maps: (a) Transverse r.e.s. ε_{yy} (b) Longitudinal r.e.s ε_{xx}.

Measurements on sample VPS 164b of W coating on surfi-sculpt steel substrate showed consistent compressive strains in the coating and complex strain distributions in the substrate (Fig 7). Tensile strain was observed for transverse direction and compressive for the longitudinal direction in the boundary regions between the coating and substrate.

4.5 In-situ tensile tests on Ti-6Al-4V alloy

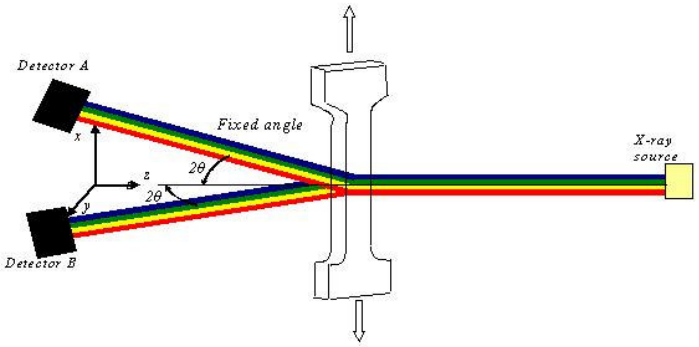

Figure 8. Experimental white beam diffraction set-up for in situ loading of Ti-6-4 dogbone specimens

To quantify the evolution of microstrain with mechanical deformation, one can measure lattice strain response by diffraction in a sample subjected to increasing uniaxial load [10]. Tensile test specimens were made from the Ti-6Al-4V alloy. The sample was mounted in the Instron universal testing machine on the high energy X-ray scattering beam line (ID15) at ESRF. In-situ loading experiment was performed in the white beam energy dispersive mode. The experimental setup is shown in Fig. 8. The sample was loaded incrementally in 500N steps and held at the prescribed load levels while diffraction data were collected.

Elastic lattice strains were obtained for crystallites oriented such that the particular *hkl* plane normal is parallel to the scattering vector, which could be chosen to be parallel (longitudinal) or perpendicular (transverse) with respect to the loading direction. Individual *hkl* reflections in the diffraction spectra were analyzed by single peak fitting to obtain the

anisotropic response of lattice planes during uniaxial tensile test. Fig. 9 shows the loading response of the lattice planes, with the normal parallel to the loading, during in situ loading. The elastic and plastic regions are indicated. Results highlight the difference in elastic and plastic response of different grain orientations via the different slope of stress-strain curves.

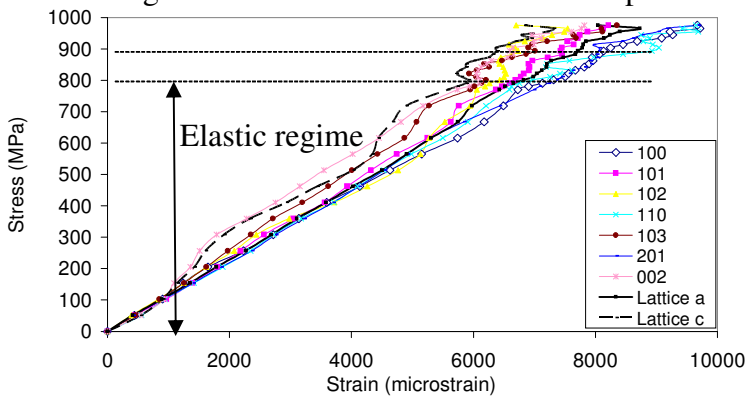

Figure 9. Stress-strain response of Ti-6Al-4V (*hkl* plane normal parallel along the applied load).

Plastic deformation affects strain mismatch between grains of different orientations [12], and diffraction peak shape, that contains a wealth of microstructural data (crystallite size and defects). A connection was confirmed between peak width and plastic strain. Fig. 10(a) shows the peak width (Full Width Half Maximum, FWHM) variation with applied load for the (110) peak. While peak width stays constant within the elastic regime, peak broadening is observed due to macro-plasticity. Peak width varies as a power function of plastic strain.

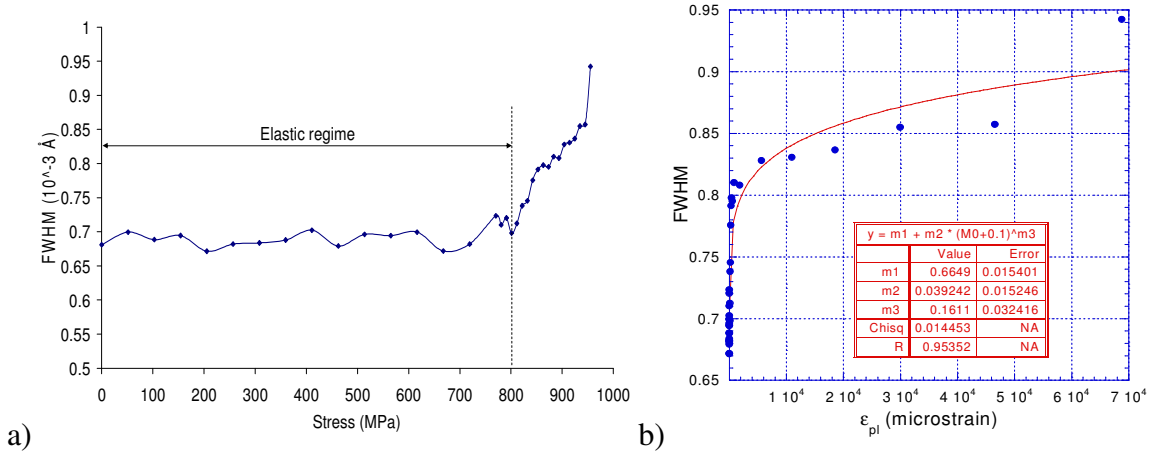

Fig. 10. (110) peak of Ti-6Al-4V: FWHM variation with a) applied stress, and b) plastic strain.

Crystal plasticity finite element (CPFE) modeling offers an excellent tool for simulating the mechanics of polycrystalline metals. Time-independent crystal plasticity constitutive equations were implemented within ABAQUS commercial FE package by Dini et al [14] showed very good agreement with experimental measurements by diffraction.

5. Conclusions

The use of white beam energy dispersive X-rays (up to and over 100keV) allows diffraction experiments in transmission through thick sections (over few mm) of important structural engineering alloys. Thus, diffraction has become an indispensable tool for residual strain/stress analysis [16]. It is now widely accepted that residual stresses and prior deformation (e.g. during fabrication) have strong influence on deformation behaviour and fatigue performance, and thus the durability of engineering structural components in service. Diffraction results can be used in predictive modelling for fatigue life prediction.

References

[1] A. Allen, M. Hutchings, C. Windsor and C. Adreani, Measurement of internal stress with bulk materials using Neutron diffraction, NDT International Oct, 1981, 249-254

[2] A.M. Korsunsky, S.P. Collins, R.A. Owen, M.R. Daymond, S. Achtioui, K.E. James (2002) "Fast residual stress mapping using energy-dispersive synchrotron X-ray diffraction on station 16.3 at the SRS." J Synchrotron Radiat, 9, p.77–81.

[3] S.Y. Zhang, W. Vorster, T. Jun, X. Song, M. Golshan, D. Laundy, M. Walsh and A. Korsunsky, "High energy white beam XRD studies of residual strains in engineering components", Proc. World Congress on Engineering, London, 2007

[4] K. Tanaka and Y. Akiniwa, "Diffraction measurements of residual macro-/microstress using X-rays, Synchrotron and Neutrons", JSME Intl J, Series A, 200, 47, pp 252–263.

[5] D. Dye, H.J. Stone, R.C. Reed, Intergranular and interphase microstresses, Current Opinion in Solid State and Materials Science 5 (2001) 31 –37.

[6] J. Liu, K. Kim, M. Golshan, D. Laundy, and A.M. Korsunsky (2005) "Energy calibration and full-pattern refinement for strain analysis using energy-dispersive and monochromatic X-ray diffraction." J. Appl. Crystallography, 38, p.661-667.

[7] P. Ballirano, R. Caminiti (2001) "Rietveld refinements on laboratory energy dispersive X-ray diffraction (EDXD) data." J Appl Crystallogr 34, p.757–762.

[8] A. Steuwer, J.R. Santisteban, M. Turski, P.J. Withers, T. Buslaps (2004) "High-resolution strain mapping in bulk samples using full-profile analysis of energy-dispersive synchrotron X-ray diffraction data." J Appl Crystallogr, 37, p.883–889.

[9] A.C. Larson, R.B. Von Dreele (2000) Gen. Structure Analysis System (GSAS) manual.

[10] D. Dye, H.J. Stone, R.C. Reed, Intergranular and interphase microstresses, Current Opinion in Solid State and Materials Science 5 (2001) 31 –37.

[11] J. Pang, T. Holden, T. Mason, "In situ generation of intergranular strains in an AI7050 alloy", Acta mater. Vol. 46, No. 5, pp. 1503-1518 (1998).

[12] X. Song, S Y Zhang, D Dini and A M. Korsunsky, Inter-granular residual stresses in polycrystalline aggregates: finite element modelling and diffraction post-processing, Materials Science Forum Vols. 571-572 (2008) pp 271-276.

[13] A. Manonukul and F. P. E. Dunne, "High- and low-cycle fatigue crack initiation using polycrystal plasticity," Proc. Roy. Soc. A, 2004.

[14] A. M. Korsunsky, D. Dini, F. P. E. Dunne, and M. J. Walsh, "Comparative assessment of dissipated energy and other fatigue criteria," Intl J. Fatigue, 29 (2007) 1990-1995.

[15] X. Song, S Y Zhang, D Dini and A M. Korsunsky, "Finite element modeling and diffraction measurement of elastic strains during tensile deformation of HCP polycrystals", to appear in the Computational Materials Science 2008.

[16] P. Withers, P. Webster, Neutron - Synchrotron X-ray strain scanning, Strain (2001) 37.